Aluminum oxide nucleation in the early stages of atomic layer deposition on epitaxial graphene

E. Schiliro, R. Lo Nigro, Se Panasci, F. M. Gelardi, S. Agnello, Rositsa Yakimova, F. Roccaforte and F. Giannazzo

Aluminum oxide nucleation in the early stages of atomic layer deposition on epitaxial graphene

E. Schilirò[1], R. Lo Nigro[1], S. E. Panasci[2,1], F. M. Gelardi[3], S. Agnello[3,1], R. Yakimova[4], F. Roccaforte[1], F. Giannazzo[1,*]

[1] *Consiglio Nazionale delle Ricerche – Istituto per la Microelettronica e Microsistemi (CNR-IMM), Strada VIII, 5 95121, Catania, Italy*

[2]*Department of Physics and Astronomy, University of Catania, Via Santa Sofia 64, 95123 Catania, Italy*

[3] *Department of Physics and Chemistry Emilio Segrè, University of Palermo, Via Archirafi 36, 90143 Palermo, Italy*

[4]*Department of Physics, Chemistry and Biology, Linköping University, Linköping SE-58183, Sweden*

*****Corresponding author. E-mail: filippo.giannazzo@imm.cnr.it (F. Giannazzo)

Abstract

In this work, the nucleation and growth mechanism of aluminum oxide (Al_2O_3) in the early stages of the direct atomic layer deposition (ALD) on monolayer epitaxial graphene (EG) on silicon carbide (4H-SiC) has been investigated by atomic force microscopy (AFM), conductive-atomic force microscopy (C-AFM) and Raman spectroscopy. Contrary to what is typically observed for other types of graphene, a large and uniform density of nucleation sites was observed in the case of EG and ascribed to the presence of the buffer layer at EG/SiC interface. The deposition process was characterized by Al_2O_3 island growth in the very early stages, followed by the formation of a continuous Al_2O_3 film (~2.4 nm thick) after only 40 ALD cycles due to the islands coalescence, and subsequent layer-by-layer growth. The electrical insulating properties of the deposited ultrathin Al_2O_3 films were demonstrated by nanoscale current mapping with C-AFM. Raman spectroscopy analyses

showed low impact of the ALD process on the defects density and doping of EG. The EG strain was also almost unaffected by the deposition in the regime of island growth and coalescence, whereas a significant increase was observed after the formation of a compact Al_2O_3 film. The obtained results can have important implications for device applications of epitaxial graphene requiring the integration of ultra-thin high-k insulators.

Keywords: Atomic layer deposition, epitaxial graphene, atomic force microscopy, Raman spectroscopy; nucleation.

1. Introduction

Due to its excellent structural, optical and electronic properties, graphene has been the object of an ever-increasing interest in the last 15 years both for fundamental studies and for a wide range of applications, including ultra-high frequency transistors [1,2], environmental or bio sensors [3] and quantum metrology standards [4]. The integration of thin insulating layers on the graphene surface represents a key step for the fabrication of graphene-based electronic devices. In particular, high-k dielectrics, such as aluminum oxide (Al_2O_3) or hafnium oxide (HfO_2) have been widely explored as gate insulators for graphene field effect transistors [1,2,5] and, more recently, as tunneling barriers of vertical hot electron transistors with a graphene base [6,7,8]. Furthermore, they can work as protective/encapsulation films or as functionalization layers for graphene-based sensors [9,10].

Deposition methods that are able to provide high quality ultra-thin insulators with conformal and uniform coating on large area are required for new-generation ultra-scaled devices. In this context, the atomic layer deposition (ALD) is the most appropriate technique to obtain films of high-k insulators with these features. In fact, due to its peculiar deposition mechanism consisting of sequential and self-limited reactions between the chemical precursors and the substrate surface, the ALD allows, in principle, a layer-by-layer growth, resulting in a linear increase of the film thickness

with the number of deposition cycles [11,12,13,14]. However, significant deviations from this ideal behavior, especially in the early stages of the deposition, can be observed in some experimental cases [15], depending on the used ALD precursors and on the specific substrate. As an example, a sub-monolayer growth per cycle can be due to steric effects from the precursors' ligands that block active sites, or to competing chemisorption pathways [15]. In the case of substrates with low density of nucleation sites, the 3D growth of islands or nanoparticles is typically observed instead of a 2D layer-by-layer growth. The 3D growth may occur either by attachment of material to the originally formed island, or by diffusion phenomena of the deposited material (adatoms and islands) [15]. In these cases, it is necessary to protract the ALD process over a large number of deposition cycles to observe the islands coalescence and the full layer formation [11,16].

Due to its planar sp^2 structure without out-of-plane bonds, graphene is an example of a surface highly unfavorable to ALD nucleation. In most of the cases, the ALD growth on graphene is very inhomogeneous, and is limited to graphene defects and edges regions [17], or in correspondence of graphene domain boundaries and wrinkles [18,19]. For these reasons, chemical pre-functionalization treatments using plasma, reactive gases [20,21] or graphene coating with different kinds of seeding-layers [22,23,24,25,26] are commonly employed to enable the ALD nucleation. Although such procedures are effective to get uniform ALD growth on graphene, they can affect, to some extent, its structural and electronic properties. Furthermore, the interfacial seed layer can be responsible for charge trapping phenomena at the dielectric/graphene interface and for an increased equivalent oxide thickness (EOT) of the seed layer/insulator stack [26]. For this reason, the direct (i.e. pre-functionalization - and seed-layer-free) ALD of insulators on graphene remains highly desirable. To date, the possibility of growing uniform high-k dielectric films directly on graphene surface by thermal ALD has been demonstrated in two specific cases, i.e. for CVD grown monolayer (1L) graphene residing on the native metal surface [27] and in the case of 1L epitaxial graphene (EG) on SiC(0001) [28]. The enhanced nucleation on these high quality (i.e. low defects density) graphene materials was ascribed, in part, to the peculiar properties of the graphene interface with the native

substrates and to the transparency of graphene to electric fields generated by interfacial charges or dipoles beneath graphene [29].

In particular, due to its peculiar formation mechanisms, EG obtained by thermal decomposition of SiC(0001) [30,31,32] is characterized by the presence of an interfacial carbon layer (buffer layer) having partial sp^3 hybridization with the Si face. This unique interface structure is responsible for a compressively strained EG. Moreover, the electrostatic interaction with the positively charged dangling bonds at the buffer layer/SiC interface are the cause of a high n-type doping (in the order of 10^{13} cm^{-2}) of the overlying EG. Uniform, conformal and compact Al_2O_3 layers with a thickness ~12 nm and a breakdown field of 8 MV/cm have been recently obtained directly onto 1L EG on SiC (0001) by a standard ALD at 250 °C using TMA and water as the Al precursor and co-reactant, respectively [28]. An important role for the uniform Al_2O_3 growth onto 1L EG was ascribed to the electrostatic doping induced by the buffer layer/SiC dangling bonds. In particular, according to ab-initio calculations, the n-type doping improves the adsorption energy of the water molecules, namely of the ALD co-reactant, providing a larger number of reactive sites for Al_2O_3 formation during the subsequent pulses of the Al precursor. This electrostatic effect is fairly homogeneous on the entire 1L EG surface, whereas it weakens with increasing the number of graphene layers due to the higher shielding effect from a multilayer system, resulting in a less homogenous ALD growth on the thicker EG regions [28].

Clearly, the direct ALD growth of Al_2O_3 on 1L EG can have important implications, especially for advanced electronic applications requiring the integration of ultra-thin insulating layers on top of graphene. However, the deposition of relatively thick (> 10 nm) Al_2O_3 films by direct ALD on EG has been considered so far [33], and a clear understanding of the nucleation and growth mechanisms of the Al_2O_3 films on the EG/SiC system in the early stages of the ALD process is still lacking.

In this work, the morphology evolution of Al_2O_3 deposited by ALD on 1L EG samples has been investigated over a wide range of deposition cycles (from 10 to 190). Al_2O_3 island growth from a very large density of nucleation sites was observed in the early stages of the ALD process, followed

by the formation of a continuous Al_2O_3 film (~2.4 nm thick) after only 40 cycles by coalescence of the islands. Raman spectroscopy analyses showed low impact of the direct ALD growth on the doping of EG. The native compressive strain of EG was almost unaffected by the deposition in the regime of island growth and coalescence, whereas a significant increase was observed after the formation of a compact Al_2O_3 film.

2. Experimental details

Epitaxial graphene was obtained by thermal decomposition of "nominally" on-axis 4H-SiC in a sublimation reactor at a temperature of 2000 °C and at a pressure of 900 mbar in Ar ambient. The presence of inert gas at atmospheric pressure in the reactor chamber strongly reduces the silicon sublimation rate from the SiC (0001) surface (as compared to vacuum conditions), thus allowing to raise the temperature required for graphene formation [31,32]. In particular, the high employed temperature (2000 °C) greatly enhances the mobility of carbon atoms on the SiC surface, resulting in a highly uniform monolayer EG coverage on a very large percentage (>98%) of the substrate area [31]. This high temperature sublimation process is highly reproducible [34] and, due to its high quality, the EG obtained by this approach has been employed in the last years for several applications, including high performance gas sensors [3] and quantum resistance standards [4].

The thickness uniformity of the as-grown EG was evaluated by reflectance mapping using a setup consisting of a modified micro- Raman spectrometer, as discussed in Ref. [35]. The number of layers was calculated by comparison of the reflectance values measured on bare 4H-SiC with those on SiC coated with 0L, 1L, and 2L graphene.

The Al_2O_3 films were deposited by thermal ALD processes in a PE-ALD LL SENTECH Instruments GmbH reactor, using TMA and H_2O as Al and O sources, respectively. Both TMA and H_2O precursors are delivered from the cylinders to the reactor chamber by N_2 carrier gas with a flow rate of 40 sccm. The ALD cycle consists of TMA and H_2O pulses of 0.06 s and 1 s, respectively, each of

two followed by 2s of purging pulse by N_2 to remove unreacted precursors. All ALD growths have been carried out using a deposition temperature of 250 °C and a chamber pressure of 20 Pa.

Morphological analyses were carried out by tapping mode AFM using a DI3100 equipment by Bruker with Nanoscope V electronics. Sharp silicon tips with a curvature radius of 5 nm were used for these investigations. The insulating properties of the deposited Al_2O_3 films were probed by conductive atomic force microscopy (C-AFM) measurements, performed in contact mode using Pt-coated silicon tips.

Raman spectroscopy measurements were conducted using a Bruker Senterra micro-Raman system equipped with a confocal microscope and a 532 nm excitation laser. A nominal laser power of 5 mW was applied to avoid damaging of EG. A pseudo-confocal aperture of 50×1000 μm was used for these analyses and the spectra were acquired in the range from 5 to 4428 cm^{-1} with maximum spectral resolution of 9 cm^{-1}.

3. Results and discussion

As-grown EG on 4H-SiC was preliminary characterized by reflectance mapping, providing information on the graphene thickness uniformity on large area. Fig. 1(a) reports a representative color map of the number of graphene layers distribution collected on a 20 μm × 20 μm sample area. From this map, a uniform 1L graphene coverage over ~98% of the surface area (red contrast) and ~2% coverage by isolated 2L or 3L graphene patches (yellow contrast) was evaluated.

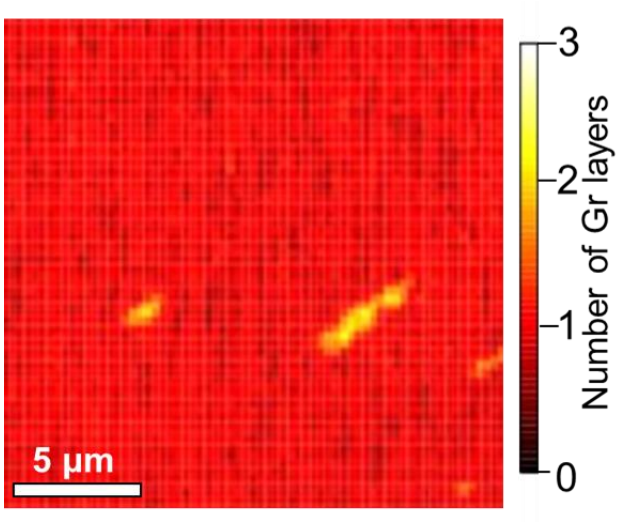

Figure 1. Number of graphene layers distribution on a 20 µm×20 µm area of EG on 4H-SiC obtained by reflectance mapping.

Al_2O_3 insulator has been grown by thermal ALD directly on pristine 1L EG surface, without any type of pre-functionalization or seeding-layer. In order to monitor the morphological evolution of the deposited Al_2O_3 from the early stages of nucleation to the formation of a continuous film, a series of depositions has been carried out with increasing number of the ALD cycles in the range from 10 to 190 cycles. Fig.2 reports four representative AFM morphologies of the as-grown EG (a) and of the deposited Al_2O_3 after 10 (d), 40 (g) and 80 (l) ALD cycles.

The as-grown EG sample exhibits a very flat surface, with large terraces separated by sub-nanometer steps associated to the 4H-SiC substrate. The low surface roughness of EG residing on the SiC terraces is also demonstrated by the representative line-scan (b) and the very narrow distribution of the height values (c), fitted with a single Gaussian peak with full-width-half-maximum (FWHM) of 0.2 nm. Fig.2(d) shows an incomplete surface coverage, with a large density of Al_2O_3 islands, in the case of the 10-cycles sample. A line-scan along the dashed red line of the AFM map is reported in Fig.2(e), from which a typical height of the Al_2O_3 islands in the order of 0.6 – 0.8 nm can be deduced. The fraction of EG surface covered by the insulator was estimated from the height distribution (Fig.2(f)) extracted from the morphology map. Such broad distribution was fitted with two Gaussian peaks, associated to the uncovered and covered EG regions, respectively. By integration of the counts under each of them, 14% and 86% percentages for the uncovered and covered areas were evaluated.

Furthermore, an average height of the Al_2O_3 highlands of 0.7 nm was deduced from the separation of the two Gaussian peaks.

As expected for the early stages of ALD processes on a sp^2 graphene surface, island growth is observed rather than an ideal layer-by-layer 2D growth. However, in the present case of 1L EG/SiC, it is worth noting a large density and uniform distribution of the Al_2O_3 islands, originating from the growth of the initial nucleation sites. This scenario is very different from the one typically observed in the cases of exfoliated or CVD graphene transferred to a substrate, where the nucleation sites are mainly localized on the edges, on structural defects or on the wrinkle regions. The high and uniform density of nucleation sites in the case of 1L EG can be ascribed to the homogeneously distributed electrostatic forces generated by the buffer layer at EG/SiC interface [28].

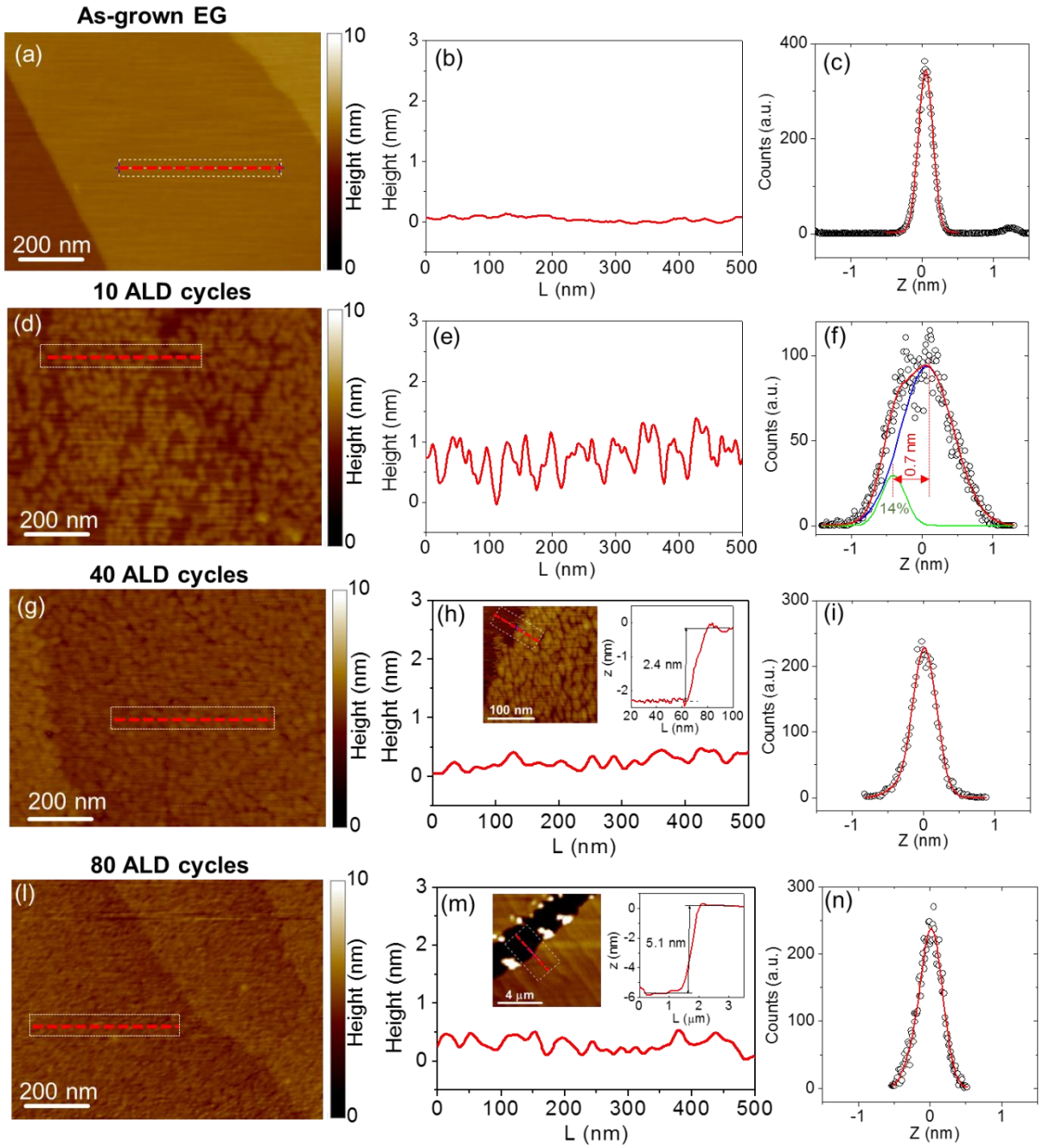

Figure 2. AFM morphology of the as-grown EG surface (a) and after 10 (d), 40 (g) and 80 (l) ALD cycles for the Al_2O_3 deposition. Representative height line-scans for the as-grown (b), 10-cycles (e), 40-cycles (h) and 80-cycles (m) sample. An incomplete coverage by Al_2O_3 islands with typical 0.6-0.8 nm height is observed after 10 ALD cycles. Closed Al_2O_3 layers are obtained after 40 and 80 ALD cycles. Distributions of the height values extracted from the morphology maps for the as-grown (c), 10-cycles (f), 40-cycles (i) and 80-cycles (n) sample.

Fig.2(g) shows that, after only 40 ALD cycles, the full coverage of the EG surface was achieved due the coalescence of the Al_2O_3 islands. A much smoother morphology than for the 10-cycles sample

can be deduced from the representative line profile in Fig.2(h) and from the narrower height distribution in Fig.2(i), fitted with a single Gaussian peak with FWHM of 0.33 nm. The deposited Al_2O_3 film thickness (~2.4 nm) was estimated in this case by measuring the step height of an intentionally scratched region, as illustrated in the insert of Fig. 2(h).

After 80 ALD cycles, the deposited Al_2O_3 insulator reaches the properties of a compact film perfectly conformal with the atomic steps of the substrate, as shown in the AFM image in Fig.2(l). The line profile in Fig.2(m) resembles the one previously measured on the 40-cycles sample, but with a slightly smoother morphology, as deduced by the smaller FWHM=0.28 nm of the single Gaussian height distribution in Fig.2(n). This suggests the occurrence of conformal layer-by-layer growth on the Al_2O_3 film formed by island coalescence.

To evaluate the electrical insulating properties of the deposited Al_2O_3 layers, C-AFM analyses were also carried out at the different stages of the ALD deposition. Fig.3(a) and (b) show a representative surface morphology and the simultaneously collected current map of as-grown EG, taken as a reference. The two maps were acquired in contact mode, by scanning the metal tip on the EG surface while applying a DC bias (1 Volt) between the tip and a macroscopic contact deposited on the sample's front side (see the schematic reported in the insert of Fig.3(a)). Two representative line profiles of the height and of the current are also shown in Fig.3(c). The EG surface exhibits a uniform conductivity, with a small deep associated to the atomic step of the 4H-SiC substrate, as reported in previous papers [36]. Fig.3(d) and (e) show a typical morphological image and the corresponding current map measured after 10 ALD cycles. The scan was carried out in a region including a scratch intentionally performed on the Al_2O_3 film, as illustrated in the insert of Fig.3(d). An inhomogeneous coverage by Al_2O_3 islands can be deduced from the contact-mode AFM topography, similarly to what was observed in the tapping mode image in Fig.2(d). The current map provides a direct evidence of the insulating properties of these Al_2O_3 islands, whereas the uncovered EG regions appear to be conductive. The close correlation between topography and conductivity is better illustrated by the height and current line-scans in Fig.3(f), which show low current values in the peaks of the height-

profile and higher current values in the valleys and the scratched area. Moreover, an average thickness of ~0.7 nm for the Al_2O_3 islands was evaluated from the line-profile across the scratch region, which is consistent with the results of the height distribution analysis reported in Fig.2(f). The morphology and current map measured on the sample subjected to 40 ALD cycles are reported in Fig.3(g) and (h), respectively, while Fig.3(i) shows the line profiles of the height and the current signal extracted along the dashed lines in the two maps. Also in this case, the scan has been carried out in a region including a scratch of the Al_2O_3 film, intentionally performed to evaluate its thickness (~2.4 nm from the step height in Fig.3(i), upper panel). The comparison between the current maps in the Al_2O_3 covered and uncovered EG regions reveals the formation of a continuous insulating film. The small fluctuations of the injected current through this ultrathin dielectric layer are correlated to local changes in the surface roughness, as deduced from the correlation of the height and current line-profiles in Fig.3(i). Finally, Fig.3(l) and (m) report the morphology and current image on the sample subjected to 80 ALD cycles, and Fig.3(n) the line-profiles of the height and of the current across a scratched area of Al_2O_3. The formation of a homogenous insulating layer with ~5.1 nm thickness can be deduced from these analyses.

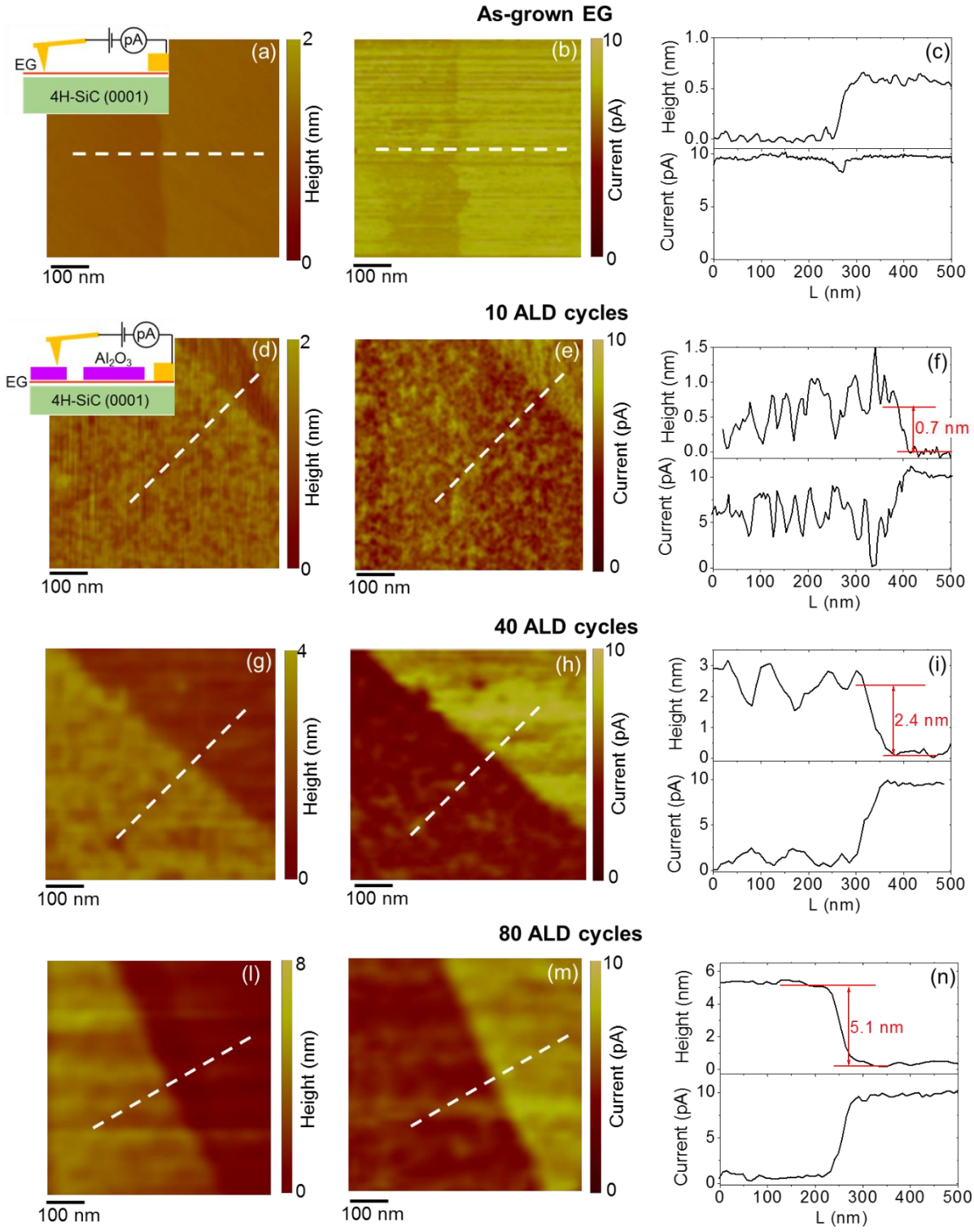

Figure 3. (a) Morphology and (b) corresponding current map (at a bias V_{tip}=1 V) measured by C-AFM on the as-grown EG surface (the experimental setup is depicted in the insert of (a)). (c) Representative line-scans of the height and of the current on the bare EG, showing a flat surface and uniform conductivity. C-AFM morphologies and current maps (at V_{tip}=1 V) after Al_2O_3 deposition with 10 ((d) and (e)), 40 ((g) and (h)) and 80 ((l) and (m)) ALD cycles. The insulating properties of Al_2O_3 are probed using the setup illustrated in the insert of panel (d). Measurements are performed close to a scratch of the Al_2O_3 film to evaluate its thickness. Line-scans of the height and of the current for the three samples are reported in the panels (f), (i) and (n).

Fig.4(a) summarizes the percentage of the covered EG surface by Al_2O_3 as a function of the number of ALD cycles. The covering level was beyond 80% already after 10 deposition cycles and full coverage (100%) was achieved after 40 deposition cycles, by coalescence of the growing Al_2O_3 islands. Fig.4(b), left scale, illustrates the increase of the Al_2O_3 island height with the number of ALD cycles in the regime of island growth (i.e. from 0 to 20 ALD cycles). Furthermore, Fig.4(b), right scale, shows the evolution of the film thickness with the number of cycles, after the formation of a continuous Al_2O_3 layer (i.e. above 40 ALD cycles). Although both the island height and the film thickness exhibit a linear increase with the number of cycles, different growth rates (evaluated as the slope of the fit) can be observed in the two regimes. This difference indicates a predominant 3D growth mechanism in the early stages of the deposition, followed by a 2D layer-by-layer growth after the formation of a continuous Al_2O_3 film (i.e. starting from 40 ALD cycles).

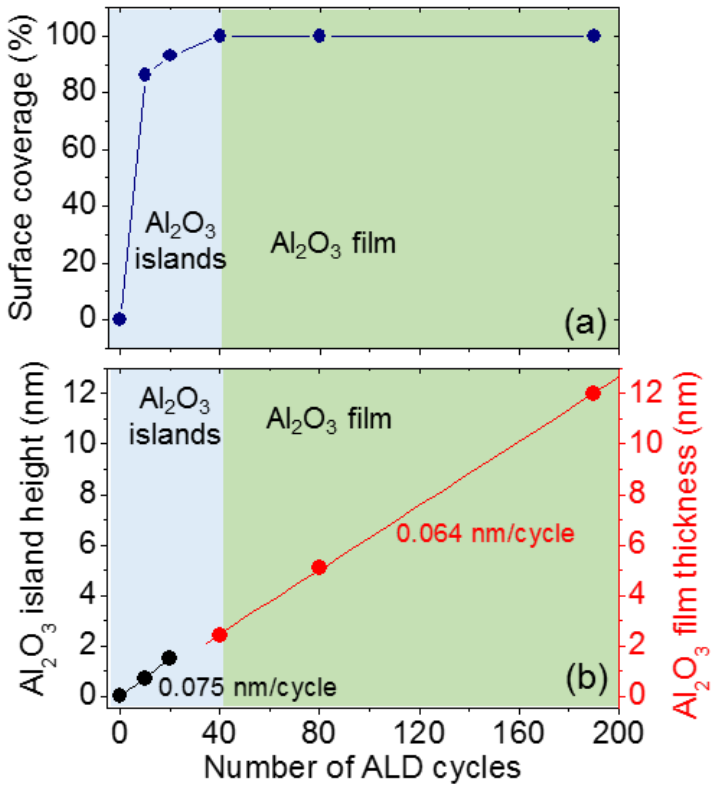

Figure 4. (a) Percentage of the EG surface covered by the deposited Al_2O_3 as a function of the number of ALD cycles. (b) Height of Al_2O_3 islands (left scale) and Al_2O_3 film thickness (right scale) versus the number of ALD cycles.

The island growth and coalescence phases have been further investigated by analyzing the evolution of the island lateral dimensions in the samples from 10 to 40 ALD cycles.

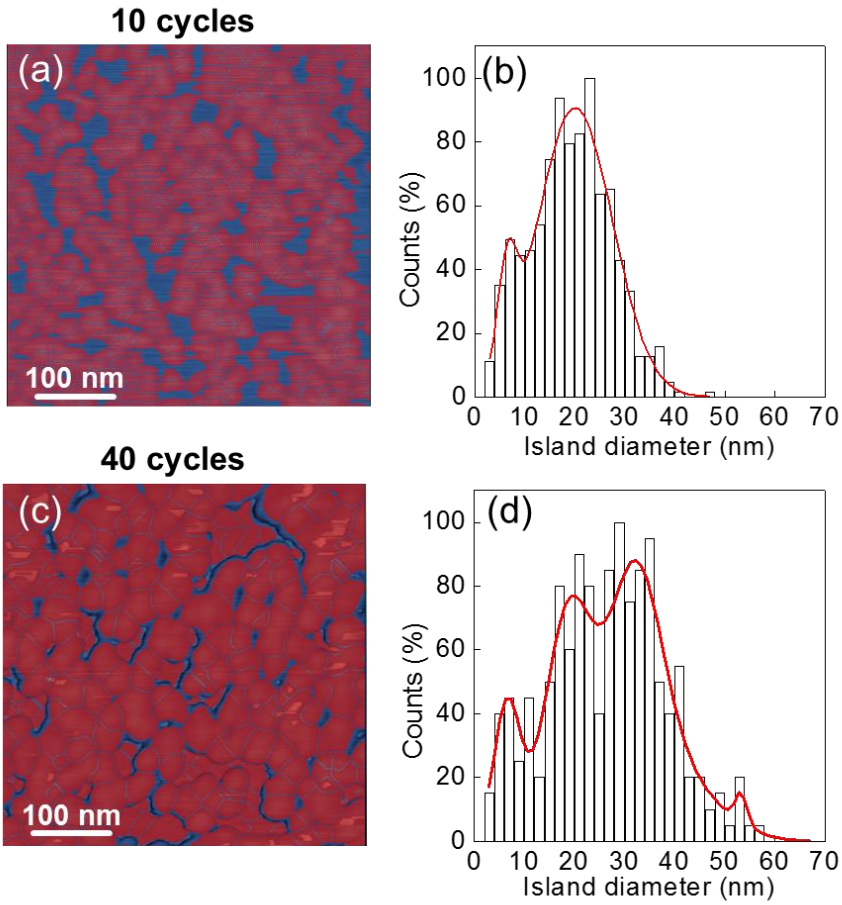

Figure 5 AFM maps for the 10 ALD cycles (a) and 40 ALD cycles (c) samples, with the contours of the Al_2O_3 islands properly highlighted to perform statistical analysis of their lateral size. Distributions of the island diameters for the 10 ALD cycles (b) and 40 ALD cycles (d) samples.

Fig.5(a) and (c) shows two representative high resolution AFM maps for the 10 and 40 cycles samples, where the island contours have been properly highlighted. The distributions of island diameters evaluated by statistical analysis of these images are reported in Fig.5(b) and (d), respectively. The 10-cycles sample (Fig.5(b)) exhibits a bimodal distribution of diameters, that has been fitted by two Gaussian peaks corresponding to 7 nm and 20 nm average island sizes. A much broader islands diameter distribution has been found for the 40-cycles sample, as illustrated by the histogram in Fig.5(d). Interestingly, the multi-peaks Gaussian fit of this distribution includes both

peaks at ~7 nm and ~20 nm (similarly to the 10-cycles sample), and further two peaks at ~30 nm and ~50 nm. This means that in the 40-cycles process there are islands of insulator further expanded on the EG substrate.

Monitoring the island size distribution during the ALD growth provides an insight into the mechanisms of nucleation and coalescence, as demonstrated in recent experimental and modeling works [37,38]. Besides the deposition parameters (temperature, precursors), the shape of the island size distribution is strongly dependent on the surface energy of the substrate. In particular, in the case of hydrophobic substrates with low surface energy, diffusion and aggregation phenomena have been shown to play an important role in the island size evolution during ALD processes [39]. In the specific case of graphene, where physisorption is the main adsorption mechanism during ALD nucleation, the weak interactions between adsorbed material and graphene can be the source of surface diffusion phenomena. Hence, in the early stages of the ALD process, there is a parallel deposition of atoms on the bare graphene surface and on the pre-existing islands, combined with the diffusion of atoms or entire islands and dynamic coalescence phenomena [40,41].

Based on these considerations, the evolution of the morphology of the deposited Al_2O_3 on EG can be explained according to the schematic depicted in Fig.6.

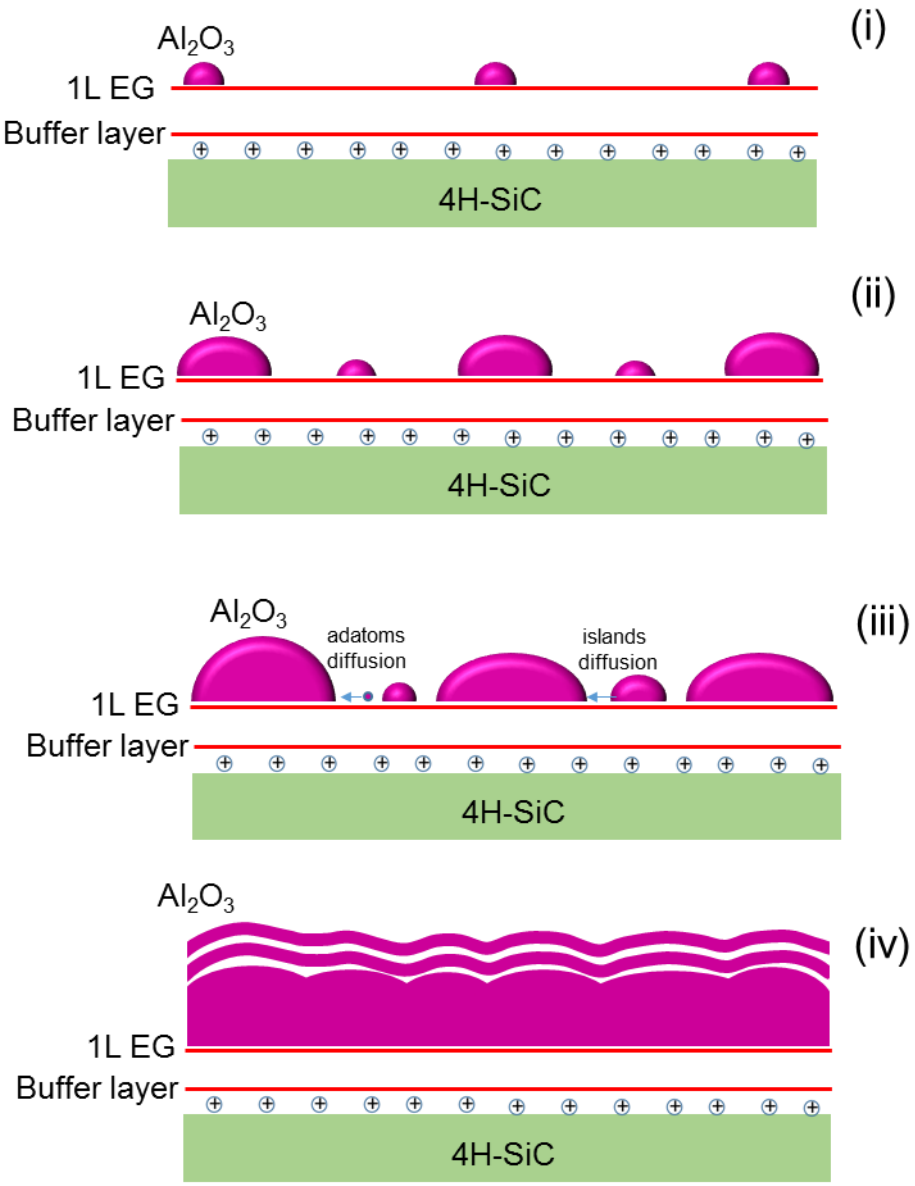

Figure 6 Schematic representation of the evolution of the deposited Al_2O_3 morphology on EG with increasing number of ALD cycles

It displays four steps of the evolution with increasing the number of ALD cycles (from top down):

(i) the formation of the first nuclei on the Graphene surface;

(ii) the adsorption of atoms on the pre-existent islands (resulting in growth both in the lateral and vertical dimensions) and the nucleation of new islands on the bare Graphene regions;

(iii) the growth of larger islands at expenses of the smaller ones (Ostwald ripening) [15] mediated by adatoms diffusion on the graphene surface, or the dynamic coalescence due to the diffusion and merging of entire islands;

(iv) the layer-by-layer ALD growth, after the formation of a continuous film on graphene.

The impact of the thermal ALD process on the doping and strain of EG has been evaluated by micro-Raman spectroscopy. Fig.7 shows a set of representative Raman spectra collected on the SiC substrate, on the as-grown EG and after Al_2O_3 deposition using an increasing number of ALD cycles (from 10 to 190).

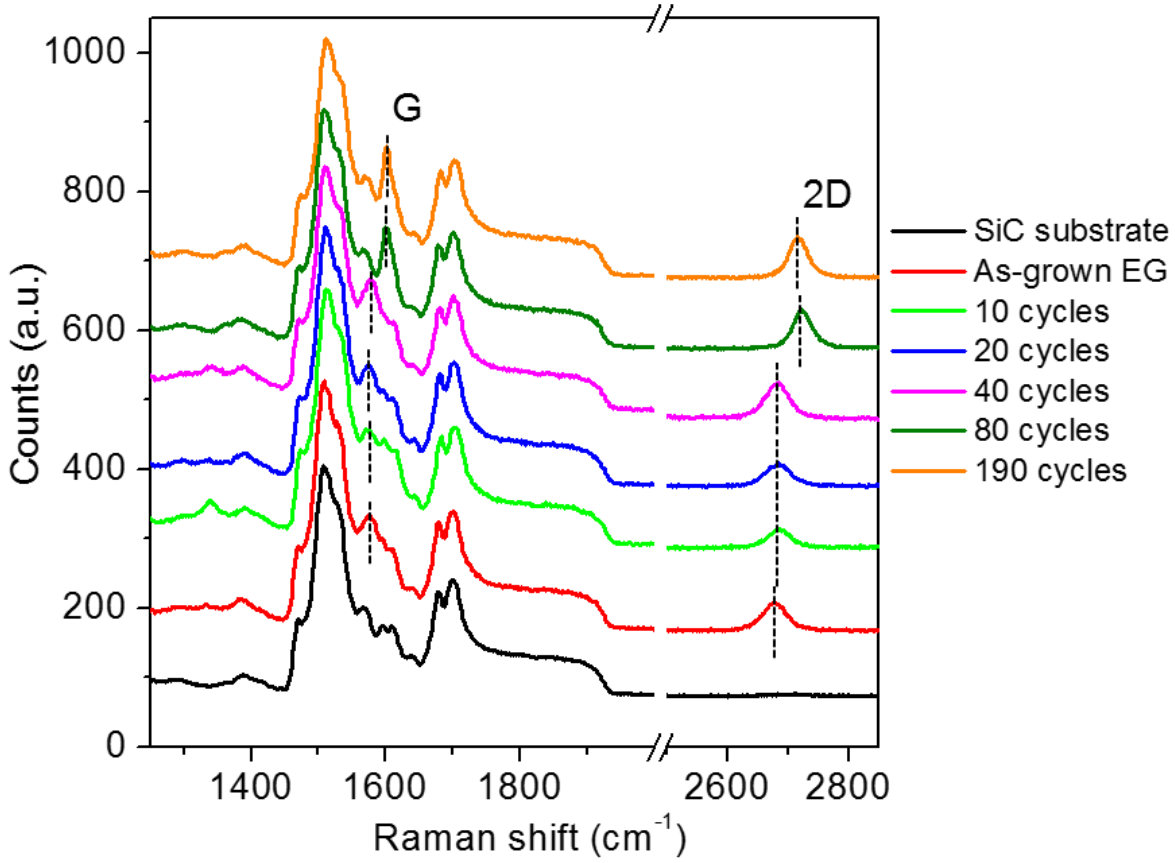

Figure 7 Raman spectra collected on the SiC substrate, on the as-grown EG and after Al_2O_3 deposition with 10, 20, 40, 80 and 190 ALD cycles. The positions of the characteristic G and 2D peaks are indicated by vertical dashed lines.

It should be noted that no specific features related to the deposited ultra-thin Al_2O_3 films are present in the considered spectral range. All the spectra have been normalized to the intensity of the Raman peak of the SiC substrate. The characteristic 2D and G peaks associated with graphitic carbon can be observed, with the G peak partially overlapping the Raman features of the SiC substrate. Noteworthy, no significant changes can be observed between the as-grown and Al_2O_3 covered EG in the D peak

spectral region (at ~1300 cm^{-1}), confirming that the ALD process does not introduce damages in EG. Furthermore, negligible shifts in the G and 2D peak positions occur moving from pristine EG up to 40 ALD cycles, whereas a significant blue shift of both peaks can be observed after 80 cycles. To better elucidate the origin of this shift, several Raman spectra have been collected at different positions on the as-grown EG samples and on all the samples with Al_2O_3 deposition at increasing number of cycles. Fig.8(a) shows a correlative plot of the 2D and G peak positions extracted from the Raman spectra on the different samples. The 2D and G positions for the ideal (i.e. strain-free and undoped) graphene ($\omega_{2D,0}$ = 2670 cm^{-1}; $\omega_{G,0}$ =1582 cm^{-1}) [42] have been also reported in the plot, along with the line describing the theoretical behavior of purely strained graphene [42] and the doping line evaluated from literature data for unstrained n-type doped graphene [43]. The dashed red lines in Fig.8(a) indicate the different graphene strain levels (from ε=-0.1% to ε=-0.5%), whereas the dashed black lines indicate the doping levels (from 1×10^{13} cm^{-2} to 3×10^{13} cm^{-2}). The point clouds for as-grown EG and for the samples with 10 to 40 ALD cycles exhibit broad distributions along the doping axis (corresponding to doping levels up to ~3×10^{13} cm^{-2}) and are almost overlapped each other. On the other hand, a narrower distribution along the doping axis (corresponding to doping levels <2×10^{13} cm^{-2}) and a shift along the strain line toward higher compressive strain values is observed after 80 and 190 ALD cycles. Fig.8(b) reports the histograms of the strain distribution for all the considered samples, evaluated from the correlative plot using the geometrical analysis described in Refs. [42,44]. Very similar broad distributions with an average compressive strain ε=-0.15% can be observed up to 40 ALD cycles, whereas a narrower distribution with the peak at ε=-0.35% is found after 80 and 190 ALD cycles. The evolution of the compressive strain as a function of the number of ALD cycles is also summarized in the plot of Fig.8(c), where the points represent the average strain values and the error bars the standard deviations for each histogram in Fig.8(b).

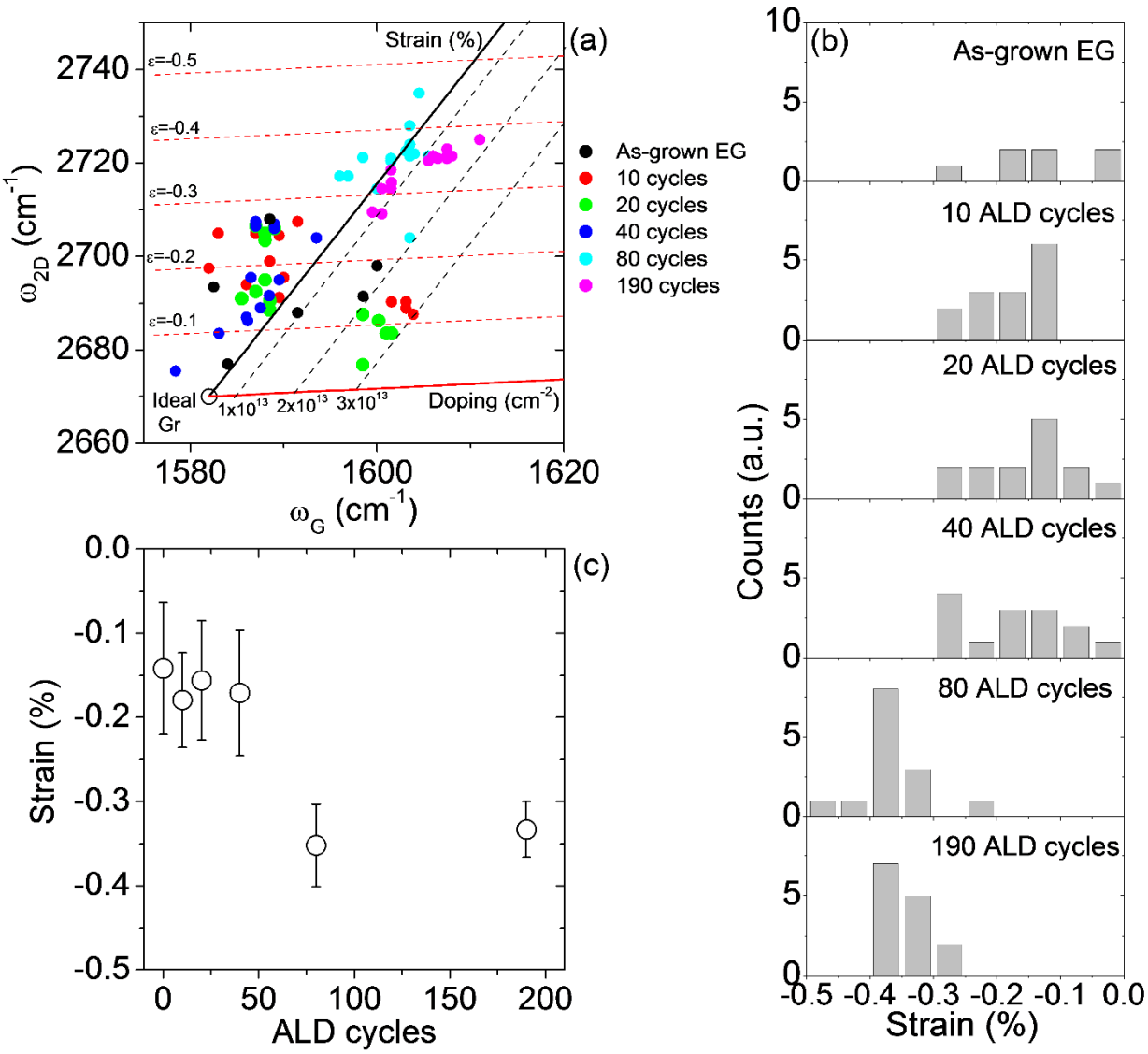

Figure 8 (a) Correlative plot of the 2D vs G peak wavenumbers (ω_{2D},ω_G) from Raman spectra collected at several positions on the as-grown EG sample and on the samples subjected to increasing number of Al_2O_3 ALD cycles. The ideal (strain-free and undoped) graphene is represented by the point ($\omega_{2D,0}$ = 2670 cm^{-1}, $\omega_{G,0}$ =1582 cm^{-1}). The theoretical strain line (black) and the doping line for n-type graphene (red) are also reported in the plot. (b) Histograms of the strain values for all the considered samples evaluated by the correlative plot. (c) Evolution of the compressive strain as a function of the number of ALD cycles.

Such a behavior, deduced from the analysis of the characteristic graphene Raman peaks, is consistent with the nanoscale resolution morphological analyses by AFM. In particular, the native compressive strain of EG appears to be almost unaffected by the early stages of the ALD process, i.e. during the nucleation and growth of Al_2O_3 islands, when the insulating film coverage is still incomplete. No significant strain variations are observed also after 40 ALD cycles, when the AFM analyses showed

full coverage of EG with a ~2.4 nm Al_2O_3 film obtained from the coalescence of Al_2O_3 islands. This indicates that the insulating film was still not compact enough to influence the strain of the underlying EG. Finally, the factor of two increase of the compressive strain after 80 ALD cycles indicates that the Al_2O_3 film (with 5.1 nm thickness) reached a compact structure, resulting in the deformation of the ultrathin graphene layer underneath. Such increased compressive strain probably accumulates after the formation of the compact Al_2O_3 film, i.e. during the cooling down step of the ALD process, as a result of the interplay between the negative thermal expansion coefficient of monolayer graphene (ranging from -3×10^{-6} K^{-1} at 250 °C to -4×10^{-6} K^{-1} at room temperature) [45] with the positive thermal expansion coefficient of Al_2O_3 (ranging from 17×10^{-6} K^{-1} at 250 °C to $\kappa\approx14\times10^{-6}$ K^{-1} at room temperature) [46]. Noteworthy, after the insulator/EG structure is stabilized, no further increase in the compressive strain is observed for larger number of ALD cycles.

4. Conclusion

In conclusion, the ALD nucleation and growth mechanisms of ultra-thin Al_2O_3 films on monolayer EG on silicon carbide (4H-SiC) has been investigated in details by morphological analyses. Island growth from a large and uniform density of nucleation sites was observed in the early stages of the deposition, followed by the formation of a continuous Al_2O_3 film (~2.4 nm thick) due to the islands coalescence after only 40 ALD cycles. Afterwards, layer-by-layer growth giving rise to a conformal and compact Al_2O_3 film was observed. The electrical insulating properties of the deposited ultrathin Al_2O_3 films were demonstrated by nanoscale current mapping with C-AFM. Raman spectroscopy analyses showed low impact of the ALD process on the defect's density and on the average doping of EG. The compressive strain of as-grown EG (ε=-0.15%) was also almost unaffected during the nucleation, growth and coalescence of Al_2O_3 islands, whereas an increase of the strain by more than a factor of two (ε=-0.35%) was observed after the formation of a compact Al_2O_3 film. The obtained results can have important implications for device applications of epitaxial graphene.

Acknowledgments

The authors acknowledge S. Di Franco from CNR-IMM, Catania, for his expert technical assistance with samples preparation. We are grateful to Ivan G. Ivanov from Linkoping University for providing the reflectance map. This project has been supported, in part, by MIUR in the framework of the FlagERA-JTC 2019 project ETMOS. RY is acknowledging the support by the SSF project GMT14-0077 and VR 2018-04962.

References

[1] Y.-M. Lin, C. Dimitrakopoulos, K. A. Jenkins, D. B. Farmer, H.-Y. Chiu, A. Grill, P. Avouris, 100-GHz Transistors from Wafer-Scale Epitaxial Graphene, *Science* 327 (2010) 662.

[2] Y. Wu, Y. Lin, A. A. Bol, K. A. Jenkins, F. Xia, D. B. Farmer, Y. Zhu, P. Avouris, High-Frequency, Scaled Graphene Transistors on Diamond-Like Carbon, *Nature* 472 (2011) 74–78.

[3] C. Melios, V. Panchal, K. Edmonds, A. Lartsev, R. Yakimova, O. Kazakova, Detection of Ultralow Concentration NO_2 in Complex Environment Using Epitaxial Graphene Sensors, ACS Sens. 3 (2018) 1666−1674.

[4] A. Tzalenchuk, S. Lara-Avila, A. Kalaboukhov, S. Paolillo, M. Syvajarvi, R. Yakimova, O. Kazakova, T.J.B.M.Janssen, V. Fal'ko, and S. Kubatkin, Towards a quantum resistance standard based on epitaxial graphene, *Nature Nanotechnology* 5 (2010) 186-189.

[5] G. Fisichella, S. Lo Verso, S. Di Marco, V. Vinciguerra, E. Schilirò, S. Di Franco, R. Lo Nigro, F. Roccaforte, A. Zurutuza, A. Centeno, S. Ravesi, F. Giannazzo, Advances in the fabrication of graphene transistors on flexible substrates. *Beilstein Journal of Nanotechnology* 8 (2017) 467-474.

[6] W. Mehr, J. Dabrowski, J. C. Scheytt, G. Lippert, Y. H. Xie, M. C. Lemme, M. Ostling, G. Lupina, Vertical Graphene Base Transistor, *IEEE Electron Device Lett.* 33 (2012) 691–693.

[7] F. Giannazzo, G. Greco, E. Schilirò, R. Lo Nigro, I. Deretzis, A. La Magna, F. Roccaforte, F. Iucolano, S. Ravesi, E. Frayssinet, et al. High-Performance Graphene/AlGaN/GaN Schottky Junctions for Hot Electron Transistors. *ACS Appl. Electron. Mater.* 1 (2019) 2342–2354.

[8] F. Giannazzo, G. Greco, F. Roccaforte, S. S. Sonde, Vertical Transistors Based on 2D Materials: Status and Prospects.Crystals 8 (2018) 70.

[9] A. A. Sagade, D. Neumaier, D. Schall, M. Otto, A. Pesquera, A. Centeno, A. Z. Elorza, H. Kurz, Highly Air Stable Passivation of Graphene Based Field Effect Devices, *Nanoscale* 7 (2015) 3558−64.

[10] T.-E. Bae, H. Kim, J. Jung, W.-J. Cho, Fabrication of High- Performance Graphene Field-Effect Transistor with Solution-Processed Al_2O_3 Sensing Membrane, *Appl. Phys. Lett.* 104 (2014) 153506.

[11] R. L. Puurunen, Surface chemistry of atomic layer deposition: A case study for the trimethylaluminum/water process, *J. Appl. Phys.* 97 (2005) 121301.

[12] S. M. George, Atomic layer deposition: an overview, *Chem. Rev.* 110 (2009) 111–31

[13] A. Pakkala, M. Putkonen, in Handb. *Depos. Technol. Film. Coatings, Elsevier*, **2010**, pp. 364–391.

[14] L. Niinistö, J. Päiväsaari, J. Niinistö, M. Putkonen, M. Nieminen, Advanced electronic and optoelectronic materials by Atomic Layer Deposition: An overview with special emphasis on recent progress in processing of high-*k* dielectrics and other oxide materials, *Phys. Stat. Sol. A* 201 (2004) 1443-1452.

[15] N. E. Richey, C. de Paula, S. F. Bent, Understanding chemical and physical mechanisms in atomic layer deposition, *J. Chem. Phys.* 152 (2020) 040902.

[16] R. L. Puurunen, W. Vandervorst, *J. Appl. Phys.* 96 (2004) 7686

[17] X. Wang, S.M. Tabakman, H. Dai, Atomic Layer Deposition of Metal Oxides on Pristine and Functionalized Graphene, *J. Am. Chem. Soc.* 130 (2008) 8152.

[18] Y. Zhang, Q. Fu, Y. Cui, R. Mu, L. Jin, X. Bao, Enhanced reactivity of graphene wrinkles and their function as nanosized gas inlets for reactions under graphene. *Phys. Chem. Chem. Phys.* **2013**, *15*, 19042.

[19] R. H. J. Vervuurt, W. M. M. Kessels, A. A. Bol,, Atomic Layer Deposition for Graphene Device Integration, *Adv. Mater. Interfaces* 4 (2017) 1700232.

[20] B. Lee, S. Park, H.-C. Kim, K. Cho, E. M. Vogel, M. J. Kim, R. M. Wallace, J. Kim, Conformal Al_2O_3 dielectric layer deposited by atomic layer deposition for graphene-based nanoelectronics, *Appl. Phys. Lett.* 92 (2008) 203102.

[21] Z. R. Robinson, G. G. Jernigan, V. D. Wheeler, S. C. Hernández, C. R. Eddy, T. R. Mowll, E. W. Ong, C. A. Ventrice, H. Geisler, I. Pletikosic, H. Yang, T. Valla, Growth and characterization of Al_2O_3 films on fluorine functionalized epitaxial graphene, *J. Appl. Phys.* 120 (2016) 075302

[22] V. K. Sangwan, D. Jariwala, S. A. Filippone, H. J. Karmel, J. E. Johns, J. M. P. Alaboson, T. J. Marks, L. J. Lauhon, M. C. Hersam, Quantitatively Enhanced Reliability and Uniformity of High‐κ Dielectrics on Graphene Enabled by Self-Assembled Seeding Layers, *Nano Lett.* 13 (2013) 1162.

[23] M. J. Hollander, M. LaBella, Z. R. Hughes, M. Zhu, K. A. Trumbull, R. Cavalero, D. W. Snyder, X. Wang, E. Hwang, S. Datta, J. A. Robinson, Enhanced Transport and Transistor Performance with Oxide Seeded High-k Gate Dielectrics on Wafer-Scale Epitaxial Graphene, *Nano Lett.* 11 (2011) 3601–3607.

[24] Y. Zhang, Z. Qiu, X. Cheng, H. Xie, H. Wang, X. Xie, Y. Yu, R. Liu, Direct Growth of High-Quality Al_2O_3 Dielectric on Graphene Layers by Low-Temperature H_2O-Based ALD, *J. Phys. D: Appl. Phys*. 47 (2014) 055106.

[25] L. Zheng, X. Cheng, D. Cao, G. Wang, Z. Wang, D. Xu, C. Xia, L. Shen, Y. Yu, D. Shen, Improvement of Al_2O_3 Films on Graphene Grown by Atomic Layer Deposition with Pre-H_2O Treatment, *ACS Appl. Mater. Interfaces* 6 (2014) 7014−7019.

[26] G. Fisichella, E. Schilirò, S. Di Franco, P. Fiorenza, R. Lo Nigro, F. Roccaforte, S. Ravesi, F. Giannazzo, Interface Electrical Properties of Al_2O_3 Thin Films on Graphene Obtained by Atomic Layer Deposition with an in Situ Seedlike Layer, *ACS Appl. Mater. Interfaces* 9 (2017) 7761-7771.

[27] B. Dlubak, P. R. Kidambi, R. S. Weatherup, S. Hofmann, J. Robertson, Substrate assisted nucleation of ultra-thin dielectric layers on graphene by atomic layer deposition, *Appl. Phys. Lett.* 100 (2012) 173113.

[28] E. Schilirò, R. Lo Nigro, F. Roccaforte, I. Deretzis, A. La Magna, A. Armano, S. Agnello, B. Pecz, I. G. Ivanov, R. Yakimova, F. Giannazzo, Seed-Layer-Free Atomic Layer Deposition of Highly Uniform Al_2O_3 Thin Films onto Monolayer Epitaxial Graphene on Silicon Carbide, *Adv. Mater. Interfaces* 1900097 (2019) 1–11.

[29] E. Schilirò, R. Lo Nigro, F. Roccaforte, F. Giannazzo, Recent Advances in Seeded and Seed-Layer-Free Atomic Layer Deposition of High-K Dielectrics on Graphene for Electronics, *C Journal of Carbon Research* 5 (2019) 53

[30] C. Berger, Z. Song, X. Li, X. Wu, N. Brown, C. Naud, D. Mayou, T. Li, J. Hass, A. N. Marchenkov, E. H. Conrad, P. N. First, W. A. De Heer, Electronic confinement and coherence in patterned epitaxial graphene. *Science* 312 (2006) 1191-1196.

[31] C. Virojanadara, M. Syvajarvi, R. Yakimova, L. I. Johansson, A. A. Zakharov, T. Balasubramanian, Homogeneous large-area graphene layer growth on 6H-SiC(0001), *Phys. Rev. B* 78 (2008) 245403.

[32] K. V. Emtsev, A. Bostwick, K. Horn, J. Jobst, G. L. Kellogg, L. Ley, J. L. McChesney, T. Ohta, S. A. Reshanov, J. Röhrl, E. Rotenberg, A. K. Schmid, D. Waldmann, H. B. Weber, T. Seyller. Towards wafer-size graphene layers by atmospheric pressure graphitization of silicon carbide, *Nature Materials* 8 (2009) 203-207.

[33] F. Giannazzo, E. Schilirò, R. Lo Nigro, F. Roccaforte, R. Yakimova, Atomic Layer Deposition of High-k Insulators on Epitaxial Graphene: A Review, Appl. Sci. 10 (2020) 2440

[34] R. Yakimova, T. Iakimov, M. Syvajarvi, Process for growth of graphene, US patent US9150417B2, 6 October 2015.

[35] I. G. Ivanov, J. Ul Hassan, T. Iakimov, A. A. Zakharov, R. Yakimova, E. Janzén, Layer number determination in graphene on SiC by reflectance mapping, *Carbon* 77 (2014) 492.

[36] F. Giannazzo, I. Deretzis, A. La Magna, F. Roccaforte, R. Yakimova, Electronic transport at monolayer-bilayer junctions in epitaxial graphene on SiC, *Phys. Rev. B* 86 (2012) 235422.

[37] F. Grillo, J. A. Moulijn, M. T. Kreutzer, J. R. van Ommen, Nanoparticle sintering in atomic layer deposition of supported catalysts: Kinetic modeling of the size distribution, *Catalysis Today* 316 (2018) 51–61

[38] F. Grillo, H. Van Bui, J. A. Moulijn, M. T. Kreutzer, J. R. van Ommen, Understanding and Controlling the Aggregative Growth of Platinum Nanoparticles in Atomic Layer Deposition: An Avenue to Size Selection, *J. Phys. Chem. Lett.* 8 (2017) 975−983.

[39] J. Soethoudt, F. Grillo, E. A. Marques, J. R. Ommen, Y. Tomczak, L. Nyns, S. Elshocht, and A. Delabie, Diffusion-Mediated Growth and Size-Dependent Nanoparticle Reactivity during Ruthenium Atomic Layer Deposition on Dielectric Substrates, *Adv. Mater. Interfaces* 5 (2018) 1800870.

[40] Y. Qi, Y. Wang, Z. Pang, Z. Dou, T. Wei, P. Gao, S. Zhang, X. Xu, Z. Chang, B. Deng, S. Chen, Z. Chen, H. Ci, R. Wang, F. Zhao, J. Yan, X. Yi, K. Liu, H. Peng, Z. Liu, L. Tong, J. Zhang, Y. Wei, J. Li, Z. Liu, Fast Growth of Strain-Free AlN on Graphene-Buffered Sapphire, *J. Am. Chem. Soc.* 140 (2018) 38.

[41] J. Dendooven, R. K. Ramachandran, E. Solano, M. Kurttepeli, L. Geerts, G. Heremans, J. Rongé, M. M. Minjauw, T. Dobbelaere, K. Devloo-Casier, J. A. Martens, A. Vantomme, S. Bals, G. Portale, A. Coati, C. Detavernier, Independent tuning of size and coverage of supported Pt nanoparticles using atomic layer deposition, *Nature Communications* 8 (2017) 1074.

[42] J. E. Lee, G. Ahn, J. Shim, Y. S. Lee, S. Ryu, Optical Separation of Mechanical Strain from Charge Doping in Graphene, *Nature Communications* 3 (2012) 1024.

[43] A. Das, S. Pisana, S. Piscanec, B. Chakraborty, S. K. Saha, U. V. Waghmare, R. Yang, H. R. Krishnamurhthy, A. K. Geim, A. C. Ferrari, A. K. Sood, Monitoring dopants by Raman scattering in an electrochemically top-gated graphene transistor, *Nature Nanotechnol.* 3 (2008) 210.

[44] F. Giannazzo, I. Shtepliuk, I. G. Ivanov, T. Iakimov, A. Kakanakova-Georgieva, E. Schilirò, P. Fiorenza, R. Yakimova, Probing the uniformity of hydrogen intercalation in quasi-free-standing epitaxial graphene on SiC by micro-Raman mapping and conductive atomic force microscopy, *Nanotechnology* 30 (2019) 284003.

[45] N. Mounet, N. Marzari, First-principles determination of the structural, vibrational and thermodynamic properties of diamond, graphite, and derivatives, *Phys. Rev. B* 71 (2005) 205214.

[46] M. Halvarsson, V. Langer, S. Vuorinen, Determination of the thermal expansion of κ-Al_20_3 by high temperature XRD, *Surface and Coatings Technology* 76-77 (1995) 358-362.